Photoacoustic measurement of the thermal properties of two-layer systems

A. M. Mansanares, A. C. Bento, and H. Vargas
Instituto de Fisica, Universidade Estadual de Campinas, 13 100 Campinas, São Paulo, Brazil

N. F. Leite and L. C. M. Miranda
Laboratorio Associado de Sensores e Materiais, Instituto de Pesquisas Espaciais, Caixa Postal 515, 12 201 São Jose dos Campos, São Paulo, Brazil

(Received 23 February 1990)

Using two different photoacoustic techniques for a two-layer system of variable thickness, we show that the thermal diffusivity and the thermal conductivity are completely determined, based upon the effective-sample model widely used in heat-transfer problems. A procedure to establish a standard photothermal technique for measuring both the thermal diffusivity and the thermal conductivity is also discussed.

I. INTRODUCTION

During the last decade, several methods have been developed to determine the thermal diffusivity with high precision by means of photothermal effects. For a review we refer to Ref. 1. The most widely used method is based upon the photoacoustic (PA) effect. The PA effect looks directly at the heat generated in a sample, due to nonradiative deexcitation processes, following the absorption of light. In the conventional experimental arrangement, a sample is enclosed in an airtight cell and exposed to a chopped light beam. As a result of the periodic heating of the sample, the pressure in the cell oscillates at the chopping frequency and can be detected by a sensitive microphone coupled to the cell. The resulting signal depends not only on the amount of heat generated in the sample (and, hence, on the optical absorption coefficient and the light-into-heat conversion efficiency of the sample) but also on how the heat diffuses through the sample. The quantity which measures the rate of heat diffusion is the thermal diffusivity, α,

$$\alpha=\frac{k}{\rho c}\ , \tag{1}$$

where k is the thermal conductivity, ρ is the density, and c is the specific heat at constant pressure. Apart from the interest in its intrinsic value, the importance of the thermal diffusivity as a physical quantity to be monitored is due to the fact that, like the optical-absorption coefficient, it is unique for each material. This can be appreciated by the tabulated values of α, given by Touloukian *et al.*[2] for a wide range of materials such as metals, minerals, foodstuffs, biological specimens, and polymers. Furthermore, the thermal diffusivity is also known to be extremely dependent upon the effects of compositional and microstructural variables,[3] as well as processing conditions as in the cases of polymers,[4–7] ceramics,[3] and glasses.[8]

The PA effect has been proved by several authors[9–13] to be a simple and reliable technique for the measurement of the thermal diffusivity. In this paper we apply two different PA detection techniques to the characterization of the thermal properties (α and k) of a two-layer system and show that, provided one of the layer constituents has their thermal properties well known, we can readily determine the thermal properties of the other constituent.

II. EFFECTIVE THERMAL DIFFUSIVITY

Consider the two-layer system shown schematically in Fig. 1(a) consisting of a material 1 of thickness l_1 and of a

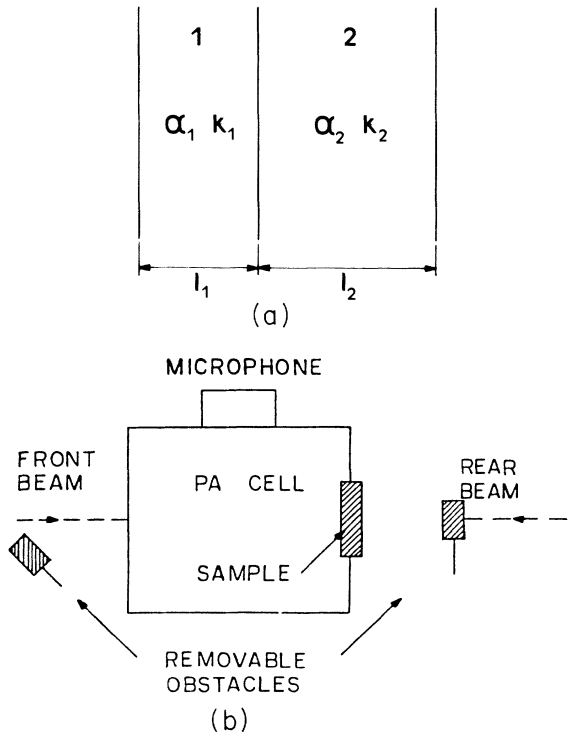

FIG. 1. (a) Geometry for the two-layer system. (b) Schematic arrangement for the two-beam photoacoustic measurement of the thermal diffusivity.

material 2 with thickness l_2, both having the same cross section. Let $l=l_1+l_2$ denote the total sample thickness, α_i the thermal diffusivity, ρ_i the density, c_i the specific heat, and k_i the thermal conductivity of material i ($i=1,2$). From the analogy between thermal and electrical resistances widely used in heat-transfer problems,[14] the effective thermal resistance R of this series two-layer system may be written as

$$R=\frac{l}{k}=R_1+R_2 , \tag{2}$$

where k is the effective thermal conductivity of the composite sample, and $R_i=l_i/k_i$ is the thermal resistance of layer i. From Eq. (2) one gets

$$k=\frac{lk_1k_2}{l_1k_2+l_2k_1} . \tag{3}$$

On the other hand, the effective heat capacity $V\rho c$ of the composite sample is given by

$$V\rho c=V_1\rho_1c_1+V_2\rho_2c_2 . \tag{4}$$

Substituting Eqs. (3) and (4) into Eq. (1) and performing some straightforward algebra, we can write the thermal diffusivity of the two-layer system as

$$\alpha=\frac{1}{\dfrac{x^2}{\alpha_1}+\dfrac{(1-x)^2}{\alpha_2}+x(1-x)\left[\dfrac{\lambda}{\alpha_1}+\dfrac{1}{\lambda\alpha_2}\right]} , \tag{5}$$

where $x=l_1/l$ measures the thickness fraction of material 1 in the composite sample, and $\lambda=k_1/k_2$. Equation (5) implies that the thermal diffusivity of the composite sample depends not only on the thermal diffusivity of its constituent materials but also on the ratio of their thermal conductivities. In Fig. 2 we show the behavior of α on the parameter x for several values of the ratio λ. The simulation, shown in Fig. 2 was carried out for a two-layer system having $\alpha_1=0.0045$ cm^2/s and $\alpha_2=0.0009$ cm^2/s which are appropriate for plate glass and poly(ethylene terephthalate) (Mylar). Figure 2 shows that on increasing λ the curve for α rises up, reaches a shape at a given value of λ, λ_c, such that the area below it is maximum [i.e., $A(\lambda)=\int_0^1 dx\,\alpha(x,\lambda)$ is maximum], and, on further increasing λ above λ_c, it gets lower and shallower again. In Fig. 3 we show the integrated value $A(\lambda)$ of $\alpha(x,\lambda)$ over the entire sample thickness as a function of λ for the above values of α_1 and α_2. It can be shown that the critical value of λ which maximizes the area $A(\lambda)$ is such that $\lambda_c=(\alpha_1/\alpha_2)^{1/2}$ or, in terms of the thermal effusivities $e_i=(k_i\rho_ic_i)^{1/2}$, when

$$e_1=e_2 . \tag{6}$$

In other words, when the thermal effusivities of the sample constituents are equal, the variation of α with respect to the thickness of layer 1 is the steepest one. In this case, the effective thermal diffusivity reduces to

$$\alpha=\frac{1}{\dfrac{x^2}{\alpha_1}+\dfrac{(1-x)^2}{\alpha_2}+\dfrac{2x(1-x)}{\sqrt{\alpha_1}\sqrt{\alpha_2}}} \tag{7}$$

or

$$\frac{l}{\sqrt{\alpha}}=\frac{l_1}{\sqrt{\alpha_1}}+\frac{l_2}{\sqrt{\alpha_2}} .$$

It should be mentioned that in a recent paper, Tominaga and Ito[15] arrived at Eq. (7) for the effective thermal diffusivity for a two-layer system. These authors reached this conclusion by applying the Rosencwaig-Gersho (RG) model to a two-layer system under rear illumination and

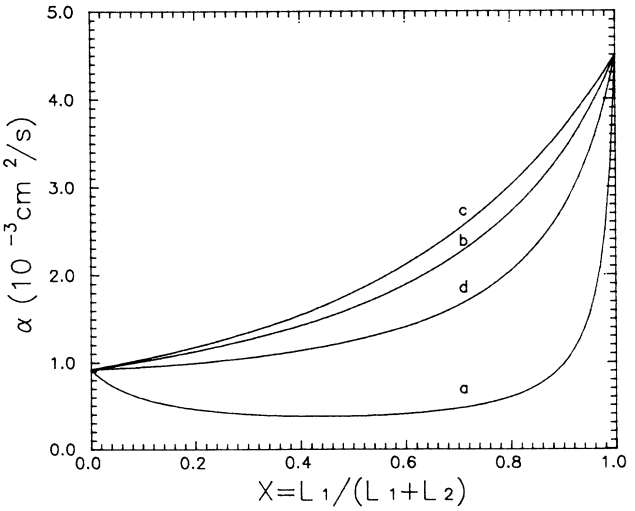

FIG. 2. Dependence of the effective thermal diffusivity of a two-layer system having $\alpha_1=0.0045$ cm^2/s and $\alpha_2=0.0009$ cm^2/s, as a function of the parameter x, for several values of λ: (*a*) $\lambda=0.1$, (*b*) $\lambda=1.0$, (*c*) $\lambda=2.24$, and (*d*) $\lambda=8.0$.

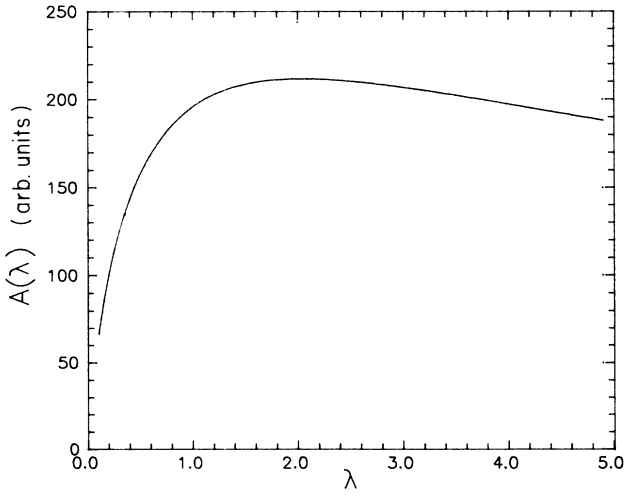

FIG. 3. Integrated value $A(\lambda)$ of the effective thermal diffusivity, as given by Eq. (5) of the text, over the entire range of x, as a function of the parameter λ. The two-layer system considered has $\alpha_1=0.0045$ cm^2/s and $\alpha_2=0.0009$ cm^2/s.

looking at the phase angle behavior as a function of the modulation frequency. They showed that, at high modulation frequencies, the rear-illumination phase angle varies as

$$\phi_R = \left[\frac{1}{\sqrt{f_1}} + \frac{1}{\sqrt{f_2}}\right]\sqrt{f} \ , \tag{8}$$

where $f_i = \alpha_i/\pi l_i^2$ is the critical frequency above which the material i becomes thermally thick. These authors then wrote ϕ_R as $\sqrt{f/f_c}$, where $f_c = \alpha/\pi l^2$, to conclude that the thermal diffusivity of the combined system is given by Eq. (7). This is an operational definition and not a deduction from first principles. It fails to reproduce the experimental results, except for a particular system such that $e_1 = e_2$. In fact, as was shown above, the thermal diffusivity of a composite system should depend explicitly on α_1, α_2, and the ratio k_1/k_2. In the next sections, we demonstrate experimentally the validity of Eq. (5) as the adequate definition of the thermal diffusivity of a series two-layer system.

III. PHASE-LAG METHOD RESULTS

In Ref. 13 we demonstrated the usefulness of a single modulation frequency method for measuring the thermal diffusivity of solid samples. The method consists of measuring the relative phase lag $\Delta\phi = \phi_F - \phi_R$ at a single modulation frequency, between the rear-surface illumination (R) and the front-surface illumination (F), as follows. Using the thermal diffusion model of Rosencwaig and Gersho[16] for the production of the PA signal, the ratio of the signal amplitude, S_F/S_R, and the phase lag for front- and rear-surface illuminations, $\Delta\phi$, are given by[13] [c.f., Fig. 1(b)]

$$\frac{S_F}{S_R} = \frac{I_F}{I_R}[\cosh^2(la_s) - \sin^2(la_s)]^{1/2} \tag{9}$$

and

$$\tan(\Delta\phi) = \tanh(la_s)\tan(la_s) \ , \tag{10}$$

where I_F and I_R are the absorbed light intensity for front and rear illumination, l is the sample thickness, and $a_s = (\pi f/\alpha)^{1/2}$ is the sample thermal diffusion coefficient. In arriving at Eqs. (9) and (10) we have assumed that the sample is optically opaque to the incident light (i.e., all the incident light is absorbed at the surface) and that the heat flux into the surrounding air is negligible. In principle, either Eq. (9) or Eq. (10) would give us the value of α from a single modulation frequency measurement. However, since Eq. (9) depends explicitly on the ratio I_F/I_R (i.e., precise power monitoring of each beam and identical surface conditions on each side of the sample are needed), the value of the thermal diffusivity in the signal amplitude ratio measurement is obtained from the slope of the curve S_F/S_R as a function of the modulation frequency. In contrast, Eq. (10) exhibits no explicit dependence on the absorbed power and surface conditions so that a single modulation frequency measurement is sufficient to derive the thermal diffusivity. Furthermore, the fact that the phase-lag method is independent of power calibrations and surface conditions renders it a more precise technique than the amplitude ratio method.

To test the above model for the effective thermal diffusivity of a series of two-layer system we have applied the PA phase-lag method to plate-glass–Mylar samples of variable constituent layer thicknesses. The thin plate glass has a fixed 150-μm thickness, whereas the Mylar sheet had variable thickness. In this way, the total thickness (and, consequently, the parameter x) of our two-layer system could be varied. The two-layer components were held together using an extremely thin layer of diffusion pump oil. The light from a 120-W tungsten lamp, after being mechanically chopped, is divided by a beam splitter and the resulting beams are directed to opposite sides of the photoacoustic cell [c.f., Fig. 1(b)]. The photoacoustic cell is a conventional brass cell in which a 0.25-in. condenser microphone (Bruel and Kjaer) is mounted in one of its walls. The samples, in the shape of 8-mm-dia disks, were flush against the back wall of the cell which has a 4-mm-dia hole through which the rear beam passes. To ensure the optical opacity implicit in Eqs. (9) and (10), a thin circular Al foil 25 μm thick and 3 mm in diameter was attached to each side of the sample using a thin layer of diffusion pump oil. As is evident from Eq. (10), the procedure to determine α is to substitute the experimental values of $\Delta\phi$ in Eq. (10) and solve it for $z = la_s$. Knowing z, the thermal diffusivity is readily given by $\alpha = \pi f(l/z)^2$. The thermal diffusivity of each constituent was measured separately, still using the PA phase-lag method, and yielded $\alpha_1 = 0.0045$ cm^2/s and $\alpha_2 = 0.000\,82$ cm^2/s for plate glass and Mylar, respectively. All the experiments were carried out in the 10–50-Hz modulation frequency range. The above values for the thermal diffusivity of plate glass and Mylar are in good agreement with the literature values given in Refs. 2 and 17, respectively. In Table I we summarize the measured values of the thermal diffusivity for our plate-glass–Mylar samples. In Fig. 4, we show the PA phase-lag data for α as a function of x. Each point in Fig. 4 represents the result of 20 experimental runs as given by our data acquisition system. The solid line in Fig. 4 represents the result of the best fit of the data to Eq. (5), leaving α_1, α_2, and λ as adjustable parameters. The data fitting procedure yielded the following values for the adjustable parameters: $\alpha_1 = 0.0045$ cm^2/s, $\alpha_2 = 0.000\,92$

TABLE I. Values of the plate-glass–Mylar system components thickness, the ratio x of the plate-glass thickness to the total system thickness, and the measured values of the thermal diffusivity, as obtained by the PA phase-lag method.

l_1 (μm)	l_2 (μm)	x	α ($\times 10^{-3}$ cm^2/s)
0	100	0.00	0.82
150	100	0.60	2.1
150	50	0.75	2.6
150	25	0.86	3.0
150	0	1.00	4.5

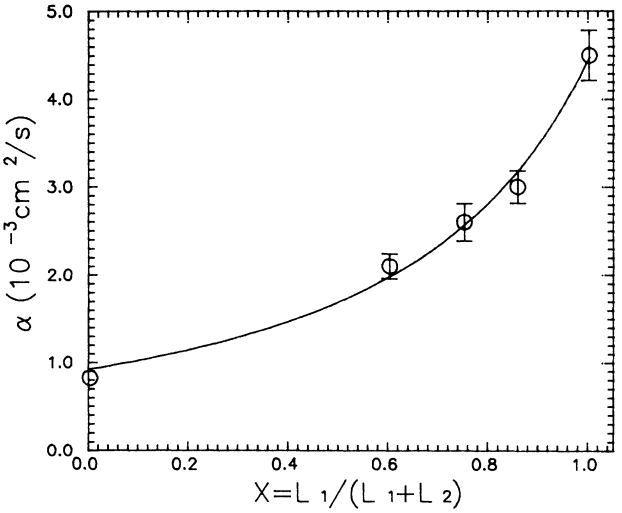

FIG. 4. Photoacoustic phase-lag obtained data for the effective thermal diffusivity of a plate-glass–Mylar system, as a function of x. The solid line represents the best fit of the data to Eq. (5) of the text.

cm^2/s, and $\lambda=3.5$. Here it should be mentioned that any best fit of α as a function of x will give us two values of λ for the same values of α_1 and α_2. This can be seen from the symmetry of the area function shown in Fig. 3. To decide which of these two values is the best one, we have introduced in the fitting procedure a criterion which express the fact that the minimum of the sum squares of the residues (SSQ) is more stable at this point. This is given by requiring that, at the best λ, the radius of curvature of the SSQ at this value of λ is the largest one. These values of α_1 and α_2 agree quite well with the measured ones. To make sure that this result for λ was the correct one, we decided to measure the thermal conductivity of our constituents.

The thermal conductivities were measured using the temperature-rise method under continuous white-light illumination. The sample were cut in the shape of 2×2 cm^2 squares and had both surfaces sprayed with black paint. In this way, we ensured not only a good light-absorbing surface, but also the same heat-transfer coefficient for each surface. The samples were adiabatically suspended in a Dewar which was subsequently vacuum sealed. Under these conditions the main heat-loss mechanism is the loss by radiation. The Dewar had an entrance optical glass window through which the continuous white-light beam was focused into one of the sample surfaces. On the opposite surface we had attached a thermocouple to the sample using thermal paste; in this way, the temperature evolution of the back surface could be monitored as a function of time. Care has been taken to prevent the heating light from reaching the thermocouple. Since the sample thicknesses, typically of the order of 100 μm, were much smaller than their widths (e.g., 2 cm), the simple one-dimensional heat diffusion equation with radiation losses could be applied to our experiment.

Solving the one-dimensional heat diffusion equation,[18] it can be shown that the long-term time evolution (i.e., for times greater than the heat diffusion time $\simeq l^2/\alpha$) of the back-surface temperature rise is given by

$$\Delta T=\frac{I_0\alpha\tau}{lk}(1-e^{-t/\tau}) , \tag{11}$$

where I_0 is the intensity of the incident light beam, and $\tau=lk/2\alpha H$ is the rising time. Here, $H=4\sigma T_0^3$, where σ is the Stefan-Boltzmann constant and T_0 is the ambient temperature, is the radiation heat-transfer coefficient. In Fig. 5(a), we show the back-surface temperature rise of a 170-μm-thick plate-glass sample as a function of time. Also shown in Fig. 5(a) is the temperature cooling of the

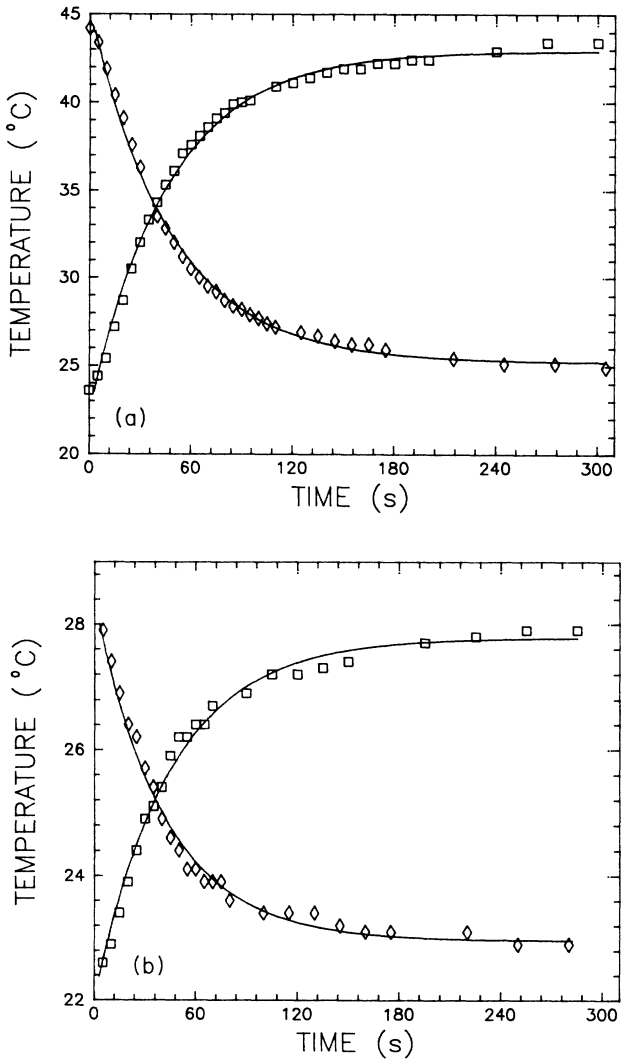

FIG. 5. (a) Back-surface temperature evolution of a 170-μ-thick black-coated plate glass as a function of time under continuous white-light illumination. The solid line represents the best fit of the data to Eq. (11) of the text. (b) Back-surface temperature evolution of a 100-μm-thick black-coated Mylar sample, as a function of time under continuous white-light illumination. The solid line represents the best fit of the data to Eq. (11) of the text.

back surface when the illumination is switched off. The solid line in Fig. 5(a) represents the result of the best fit of the experimental data to Eq. (11). From the adjusted value of τ we have then calculated the thermal conductivity for the plate-glass sample; the value obtained within a 10% error was $k_1 = 14.9$ mW/cm K. In Fig. 5(b) we show our results for the temperature evolution of the back surface of a 100-μm-thick Mylar sample. Repeating the same data fitting procedure as above, we got, for the thermal conductivity of the Mylar sample, $k_2 = 3.9$ mW/cm K. From these values of k_1 and k_2 one obtains $\lambda = 3.8$ which is in good agreement with the value of $\lambda (= 3.5)$ obtained from the effective thermal diffusivity data fitting.

IV. OPEN-PHOTOACOUSTIC-CELL RESULTS

The second test we carried out was on a two-layer system consisting of a 60-μm-thick Al foil with one of its surfaces coated with a layer of white paint of variable thickness. The paint used was a white-paint spray used in refrigerator painting. The paint-coating thickness was varied by successively spraying the white paint. The thermal diffusivity was measured using a different PA technique, namely, the so-called open-photoacoustic-cell (OPC) technique.[19,20] The schematic cross section of the OPC configuration is shown in Fig. 6. It consists of mounting the sample directly onto a circular electret microphone. It is an open-cell detection configuration in the sense that the sample is placed on top of the detection system itself, as in the case of piezoelectric and pyroelectric detections. The typical design of an electret microphone[21,22] consists of a metalized electret diaphragm (12 μm FEP with a 500–1000-Å-thick deposited metal electrode) and a metal back plate separated from the diaphragm by an air gap (45 μm long). The metal layer and the back plate are connected through a resistor R. The front sound inlet is a circular hole 3 mm in diameter, and the front air chamber adjacent to the metalized face of the diaphragm is roughly 1 mm long. As a result of the periodic heating of the sample by the absorption of modulated light, the pressure in the front chamber oscillates at the chopping frequency, causing diaphragm deflections, which generate a voltage V across the resistor R. This voltage is subsequently fed into a field-effect-transistor (FET) preamplifier already built in the microphone capsule.

Consider the schematic cross section for the electret microphone shown in Fig. 7(a), in which the electret foil has a charge density σ_0 per cm^2, dielectric constant ϵ, thickness l_m, and is separated from the metal back plate by an air gap of thickness s_1. If a sound wave impinges on the electret membrane, the thickness s_1 of the air gap is changed periodically thus changing the electric fields and inducing charges in the dielectric layers, and generating a voltage V across the resistor R. This voltage is obtained by solving the equation of motion for a circular membrane stretched with tension T over one end of a vessel (e.g., air-gap region) that is air tight. This is the so-called kettledrum model[23] for the electret microphone. Denoting by $\delta P \exp(j\omega t)$ the PA sound pressure in the front chamber causing the diaphragm deflection it can be shown that the microphone output voltage reduces to

$$V = \frac{l_b l_m \sigma_0}{l_b \epsilon + l_m \epsilon_0} \frac{j\omega RC}{1 + j\omega RC} \frac{\delta P}{\gamma P_0} \exp(j\omega t) , \tag{12}$$

where $C = A\epsilon\epsilon_0/(l_m\epsilon_0 + s_1\epsilon)$ is the capacitance of the microphone, l_b is the static back-plate air-gap thickness, γ is the specific-heat ratio, and $j = \sqrt{-1}$. To find the pres-

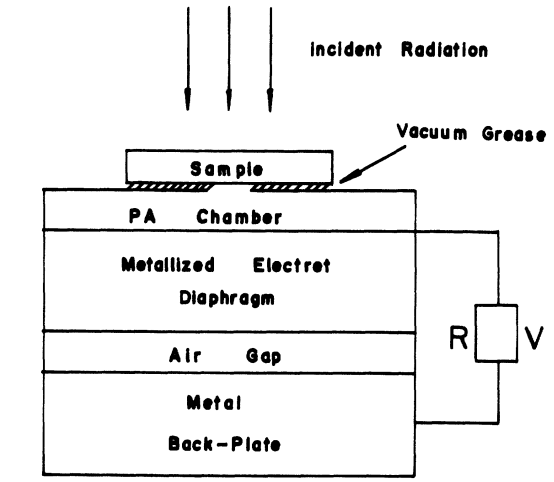

FIG. 6. Cross section of the open-photoacoustic cell using the front air chamber of a common electret microphone as the transducer medium.

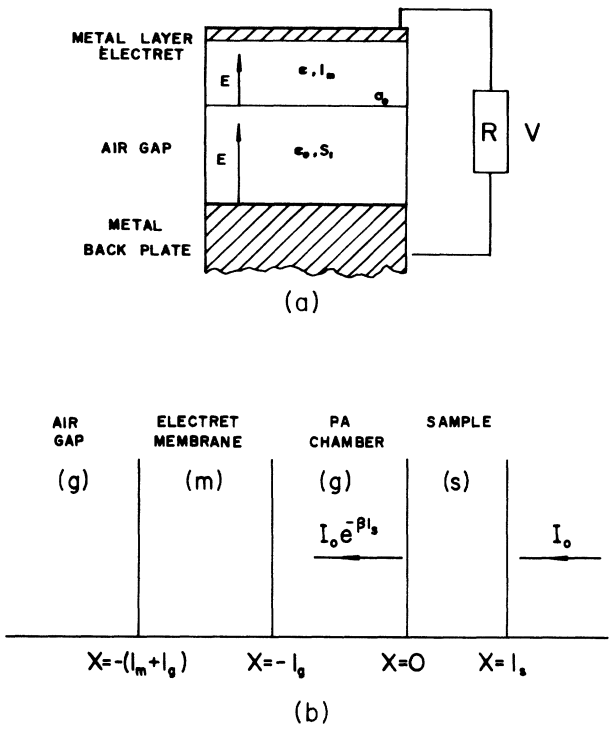

FIG. 7. (a) Cross section for the electret microphone. (b) Schematic open-photoacoustic-cell geometry.

sure fluctuation δP in the OPC configuration [Fig. 7(b)] we assume the composite thermal piston model,[24,25] according to which the total pressure fluctuation in the PA gas cell is due to three main contributions: (i) Sample-to-gas thermal diffusion. This effect is sensitive to the sample surface temperature as described by the RG model. (ii) Sample thermal expansion. This effect depends on the average sample temperature. (iii) Thermoelastic bending. This effect is essentially due to the temperature gradient inside the sample along the thickness axis (x axis). Due to the existence of this temperature gradient along the x axis, thermal expansion depends on x. This entails in an x dependence of the sample displacement along the radial direction thereby inducing a bending of the sample in the x direction. The contribution from the sample bending and dilation is formally described by the coupled set of thermoelastic equations and is described in detail in Refs. 20 and 26. It can be shown[20,26] that for samples such that its lateral dimension is much greater than its thickness, the thermoelastic bending is the dominant contribution to the vibrating sample piston. Assuming an optically opaque sample, which is appropriate for our white-paint-coated Al samples (the coated surface facing the PA chamber), and solving the thermal diffusion and thermoelastic equations as detailed in Refs. 20 and 26, the output voltage can be written as

$$V=V_0\frac{j\omega\tau_E}{1+j\omega\tau_E}\frac{\beta' I_0}{T_0 l_g\sigma_g k_s\sigma_s}\left[\frac{[1-\exp(-l_g\sigma_g)]}{\sinh(l_s a_s)}-\frac{3\mathcal{R}^4\alpha_T T_0}{2\mathcal{R}_c^2 l_s^2}\left[\frac{\alpha_s}{\alpha_g}\right]^{1/2}\frac{[l_s\sigma_s\sinh(l_s\sigma_s)-\cosh(l_s\sigma_s)+1]}{l_s\sigma_s\sinh(l_s\sigma_s)}\right]\exp(j\omega t)\ , \tag{13}$$

where $V_0=(l_b l_m\sigma_0)/(l_b\epsilon+l_m\epsilon_0)$, $\tau_E=RC$, β' is the surface absorption coefficient, $\sigma_i=(1+j)a_i$ with $a_i=(\pi f/\alpha_i)^{1/2}$ being the thermal diffusion coefficient of material i, $\mathcal{R}_c$ is the radius of the PA chamber in front of the microphone diaphragm ($\mathcal{R}_c=3.5$ mm), $\mathcal{R}$ is the support radius of the sample (i.e., the radius of the microphone front hole, $\mathcal{R}=1.5$ mm), and α_T is the sample thermal expansion coefficient. The first term in Eq. (13) is due to the air contribution whereas the second one represents the sample thermal expansion contribution. The thermal diffusivity is obtained in the OPC method by fitting the experimental data to Eq. (13) leaving α_s as an adjustable parameter.

In Fig. 8 we present OPC signal amplitude data as a function of the modulation frequency for an uncoated 60-μm-thick Al foil [curve (a)], and two 60-μm-thick Al foils coated with 23- and 88-μm-thick white-paint layers corresponding to curves (b) and (c), respectively. These data were recorded using a 250-W tungsten filament lamp whose polychromatic beam is mechanically chopped and focused onto the uncoated surface of our samples. The samples were placed on top of the electret microphone as indicated if Fig. 6. A SR 530 lock-in amplifier was used to analyze the amplitude and phase of the microphone signal, as a function of the modulation frequency. Figure 8 shows us that, for the case of the uncoated sample, the OPC signal amplitude varies as $f^{-1.5}$ for modulation frequencies greater than roughly 60 Hz, whereas for lower frequencies it exhibits a saturation-like behavior due to the microphone frequency response. The $f^{-1.5}$ frequency dependence corresponds to the expected behavior of a thermally thin sample ($l_s\sigma_s\ll 1$) when the gas thermal piston contribution, given by the first term of Eq. (13), is the dominant one. This can be readily seen from Eq. (13)

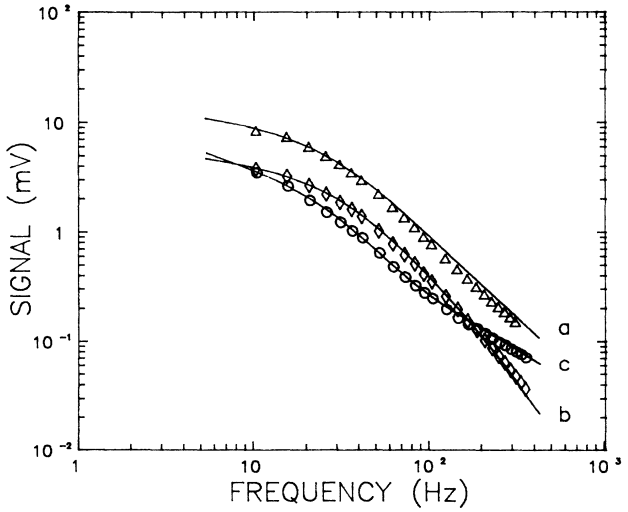

FIG. 8. OPC signal amplitude as a function of the modulation frequency for (*a*) a 60-μm-thick Al-foil sample and two 60-μm-thick Al foils coated with (*b*) 23-μm- and (c) 88-μm-thick layers of white paint. The solid lines represent the data fitting to Eq. (13) of the text.

TABLE II. Values of the white-paint-coated Al samples constituent thickness, the ratio x of the Al-foil thickness to the total sample thickness, and the measured values of the thermal diffusivity as obtained from the OPC signal amplitude data fitting.

l_1 (μm)	l_2 (μm)	x	α (cm^2/s)
60	107	0.360	0.0031
60	88	0.405	0.0029
60	54	0.526	0.0021
60	49	0.550	0.0022
60	28	0.682	0.0027
60	23	0.723	0.0041
60	14	0.811	0.0060
60	0	1.00	0.92

by setting $l_s\sigma_s \ll 1$, and neglecting the thermoelastic contribution (i.e., putting $\alpha_T = 0$). We note that a 60-μm-thick Al sample ($\alpha_s = 0.92$ cm^2/s, $k_s = 2.37$ W/cm K) is thermally thin for modulation frequencies up to roughly 8 KHz. In contrast, curve (b) in Fig. 8 exhibits an essentially exponential behavior above 60 Hz, whereas curve (c) behaves as $f^{-1.0}$ for modulation frequencies greater than 100-Hz. In other words, as the samples get thicker due to thicker paint coating, the OPC signal above 60 Hz tends to decrease initially faster [in the case of curve (b)] but then, at high modulation frequencies, it tends to scale as $f^{-1.0}$. This $f^{-1.0}$ modulation frequency dependence for rear-signal illumination is well known[4,20,26] to be due to the fact that the dominant mechanism responsible for the PA signal, in this frequency range, is the thermoelastic contribution. In fact, the relative behavior of curves (a)–(c) in Fig. 8, with respect to the paint layer thickness, is in good agreement with the one predicted by Eq. (13), as the sample becomes thermally thick with increasing thickness. Indeed, the first term in Eq. (13) predicts that, in the high-frequency range where the sample becomes thermally thick (i.e., $l_s\sigma_s \gg 1$), the signal scales as $\exp(-a\sqrt{f})/f$, where $a = l_s(\pi/\alpha_s)^{1/2}$, in contrast, the second term in Eq. (13) predicts that the signal should vary as $f^{-1.0}$. As the evidences in Fig. 8 point in the direction of a system that is changing its thermal properties α_s, k_s, and α_T with increasing paint-coating thickness, we have then decided to apply the two-layer model of Sec. II to the Al-white-paint-coated samples. This was carried out by using Eq. (13) in the best fit of the OPC signal amplitude, leaving $a = l_s(\pi/\alpha_s)^{1/2}$, τ_E, α_T, and V_0 as adjustable parameters. As in Sec. III, knowing a, the effective thermal diffusivity is readily given by $\alpha_s = \pi(l_s/a)^2$.

The solid lines in Fig. 8 correspond to the best fit of the data to the theoretical expression for the OPC signal amplitude obtained from Eq. (13). Using the adjusted values of a, we have then calculated the sample effective thermal diffusivity α, whose values are summarized in Table II. In Fig. 9 we show the OPC data for α as a function of the thickness ratio parameter x, defined as the ratio of the Al thickness to the total sample thickness. The solid line in Fig. 9 represents the result of the best fit of the thermal diffusivity data to Eq. (5), leaving α_1, α_2, and $\lambda = k_1/k_2$ as adjustable parameters. Here, the subscript 1 refers to the Al constituent. The data fitting procedure yielded the following values for the adjustable parameters: $\alpha_1 = 0.92$ cm^2/s, $\alpha_2 = 0.0030$ cm^2/s, and $\lambda = 1000$. The error in the data fitting was 0.2%. In particular, we note that the obtained value for α_1 agrees quite well with the literature value for Al. Regarding the value of α_2 corresponding to the white paint, we could not find any reported data in the literature. However, what we can say is that the above value seems to be a reasonable one since it is of the order of magnitude of most polymers. From the adjusted value of λ, using the literature value of $k_1 = 2.37$ W/cm K for Al, we have then estimated k_2 to be 2.37 mW/cm K from which we got $\rho_2 c_2 = 0.79$ J/cm^3 K for the white-paint specific heat. These values for the white-paint thermal conductivity and specific heat are both of the same order of magnitude as those of vinyl acetate and similar polymers.[17] The dashed line in Fig. 9 represents the result of the best fit of the data or Eq. (7) for α, as predicted by Tominaga and Ito. This data fitting procedure yielded the following values for the fitting parameters: $\alpha_1 = 0.92$ cm^2/s, $\alpha_2 = 0.0003$ cm^2/s. Comparing the two curves in Fig. 9 we note that the dashed curve fails to follow the experimental data except for values of x close to unity. This seems to indicate that the two-layer model of Sec. II is a more realistic description of the composite sample.

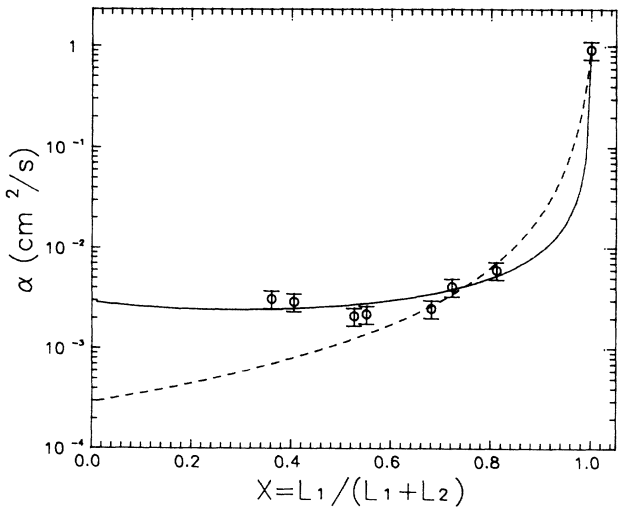

FIG. 9. Effective thermal diffusivity data as obtained from the OPC signal amplitude data fitting for the Al-white-paint samples, as a function of x. The solid and dashed curves represent the best fit of the data to Eqs. (5) and (7) of the text, respectively.

To make sure that the valence of α_2 and k_2 obtained from our two-layer model were correct, we have decided to measure the specific heat $\rho_2 c_2$. From the data fitting results we got $\rho_2 c_2 = 0.79$ J/cm^{3}K. On the other hand, the value of $\rho_2 c_2$ can be measured indirectly in two different ways. One is from the OPC signal amplitude at low frequencies where the sample is thermally thin. In this regime, the OPC signal is dominated by the gas thermal piston contribution, and it can be shown from Eq. (13) that, in this region, the OPC signal varies with the inverse of the specific heat, namely,

$$V \simeq \frac{\text{const} \times 1}{(l\rho c)_s} . \tag{14}$$

Using Eq. (4) in Eq. (14), we can write the ratio of the microphone output signal for a given sample to that of the bare Al sample, at a fixed modulation frequency, as

$$V_{\text{rel}} = \frac{1}{1 + \left[\frac{1-x}{x}\right] r} , \tag{15}$$

where $r = \rho_2 c_2/\rho_1 c_1$ is the ratio of the white-paint specific heat to the Al specific heat. In Fig. 10, we show

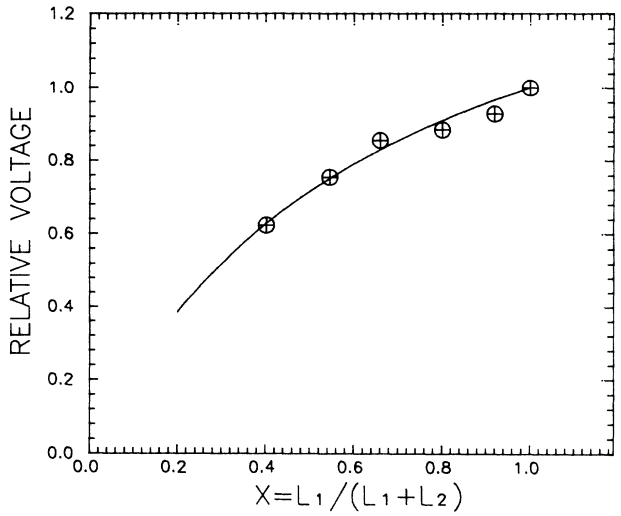

FIG. 10. Ratio of the OPC signal amplitude of the Al-white-paint samples to the OPC signal of an uncoated 60-μm-thick Al sample, recorded at 10-Hz modulation frequency using a He-Ne laser, as a function of x. The solid line represents the data fitting to Eq. (15) of the text.

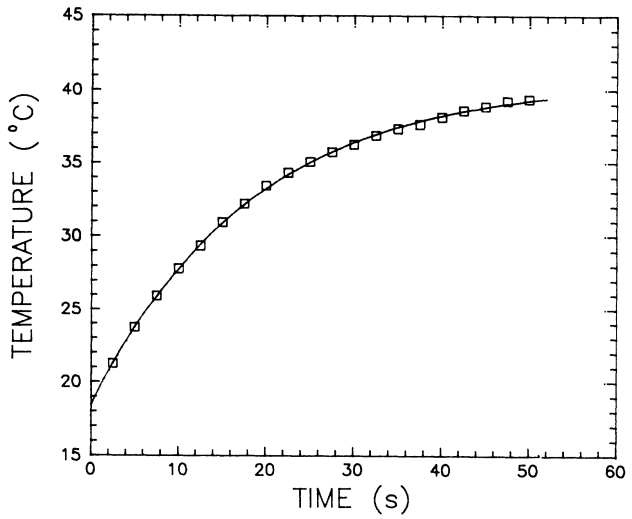

FIG. 11. Back-surface temperature evolution of a 60-μm-thick Al foil coated with a 49-μm-thick white-paint layer as a function of time under continuous white-light illumination. The solid line represents the best fit of the data to Eq. (11) of the text.

the data we got for $V_{\rm rel}$ at 10 Hz for our samples. To assure that the ratio was not affected by illumination effects, such as, illuminated area and power fluctuations, the OPC data shown in Fig. 10 were recorded using a 1.57-mW stabilized He-Ne laser source. The laser was switched on 3 h before the data were recorded. The solid line in Fig. 10 represents the best fit of the data to Eq. (15) leaving r as an adjustable parameter. The error in the fitting procedure was 2.5% and the value found for r was $r=0.40$. From this value of r, using $\rho_1 c_1=2.57$ J/cm^3 K, we got $\rho_2 c_2=1.03$ J/cm^3 K which is quite close to the one obtained above from the effective thermal diffusivity data. The second method we used to check the value of $\rho_2 c_2$ was the thermal-rise method as described in Sec. III. In this case, the rising time τ varies as $\tau \simeq (l\rho c)_s$ so that the ratio of the rising time of a given sample to that of a reference sample can be written as

$$\tau_{\rm rel}=\frac{1+r\left[\dfrac{1-x}{x}\right]}{1+r\left[\dfrac{1-x_0}{x_0}\right]}, \tag{16}$$

where r is defined as above and x_0 is the ratio parameter of the Al-white-paint reference sample. In the case of our measurements, $x_0=0.92$ since we have used as a reference sample a 60-μm-thick Al foil coated with a 5-μ-thick white-paint layer. In Fig. 11 we show a typical result of the temperature-rise measurements for a 60-μm-thick Al foil coated with a 49-μm-thick white-paint layer. The solid line in Fig. 11 is the result of the best fit of the data to Eq. (11) from which the rising time is obtained. Repeating these experiments for all the samples and calculating $\tau_{\rm rel}$, as given by Eq. (16), we have then found the parameter r from the $\tau_{\rm rel}$ data fitting which leads us to estimate $\rho_2 c_2$ to be 1.08 J/cm^3 K. This value agrees with the one obtained from $V_{\rm rel}$ data and is again close to the one obtained from the thermal diffusivity measurements.

Finally, in Fig. 12 and Table III we present the results for the thermal expansion coefficient we got from the OPC signal amplitude data fitting, as a function of the ratio parameter x. Figure 12 tells us that on increasing the paint layer thickness, the thermal expansion coefficient also increases. It eventually reaches a saturation when the paint layer is sufficiently thick. This increase of α_T with increasing paint thickness explains the observed $f^{-1.0}$ modulation dependence as well as the role played by the thermoelastic bending in the OPC signal amplitude data of Fig. 8. The solid line in Fig. 12 represents

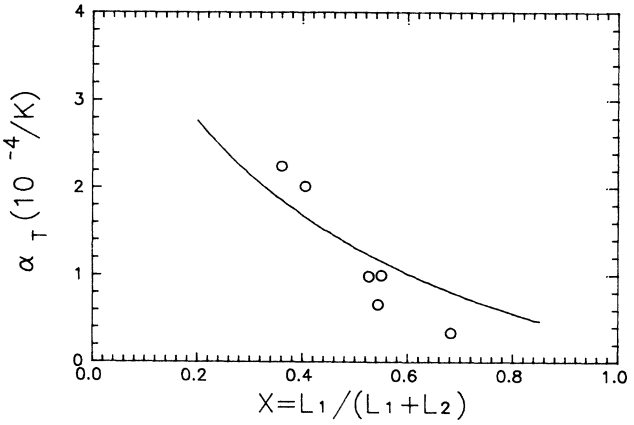

FIG. 12. Effective thermal expansion coefficient as obtained from the OPC signal amplitude data fitting for the Al-white-paint samples, as a function of x. The solid curve represents the data fitting to Eq. (18) of the text.

TABLE III. Values of the white-paint-coated Al sample constituent thickness, the ratio of x of the Al-foil thickness to the total sample thickness, and the thermal expansion coefficient as obtained from the OPC signal amplitude data fitting.

l_1 (μm)	l_2 (μm)	x	α_T ($\times 10^{-4}$ K^{-1})
60	107	0.360	2.25
60	88	0.405	2.01
60	54	0.526	0.985
60	50	0.545	0.664
60	49	0.550	0.997
60	28	0.682	0.337

the best fit of the data to the theoretical expression for α_T as predicted by the effective sample model. This, in turn, is derived from the model developed in Sec. II as follows. From Eq. (4) one has

$$\delta l\, \rho c = \delta l_1 \rho_1 c_1 + \delta l_2 \rho_2 c_2 \ . \tag{17}$$

Writing $\delta l = \alpha_T \Delta T\, l$ and $\delta l_i = \alpha_{Ti} \Delta T\, l_i$, and using Eqs. (3) and (5), one finds from Eq. (17)

$$\alpha_T = \alpha_{T1} \frac{x^2 + x(1-x)(\lambda+\zeta) + \lambda\zeta(1-x)^2}{x^2 + \gamma(1-x)^2 + x(1-x)\left[\lambda + \dfrac{\gamma}{\lambda}\right]} \ , \tag{18}$$

where α_{Ti} is the thermal expansion coefficient of material i, λ is the ratio of the thermal conductivities of materials 1 and 2 as defined in Sec. II,

$$\zeta = (\alpha_{T2}/\alpha_{T1})(\rho_2 c_2/\rho_1 c_1) \ ,$$

and $\gamma = \alpha_1/\alpha_2$. Equation (18) has, in principle, four adjustable parameters. However, from the thermal diffusivity data fitting, two of them, λ and γ, were already determined, namely, $\lambda = 1000$ and $\gamma = 307$, at the same time that the thermal expansion coefficient for Al is well known, $\alpha_{T1} = 0.000\,023$ K^{-1}. We are thus left just with one adjustable parameter, namely, ζ. The result we got was $\zeta = 6.46$, which gives us $\alpha_{T2} = 0.000\,48$ K^{-1} for the white-paint thermal expansion coefficient. This value of α_{T2} is in reasonable agreement[27] with the ones of most rubberlike polymers, polyvinyl butyral and cellulose nitrate.

V. CONCLUSIONS

In this paper we have discussed the photoacoustic measurements of the thermal properties of two layers in series systems. The measurements were carried out using two different detection techniques on two different layered samples. One type of sample (i.e., the plate-glass–Mylar system) was made of materials having thermal properties relatively close to each other, whereas in the second sample tested the constituent materials had their thermal diffusivities and conductivities varying several orders of magnitudes (i.e., the white-paint-coated Al-foil sample). The PA detection techniques used were the phase-lag technique and the open-photoacoustic-cell technique so that the thermal diffusivity could be obtained from both the PA signal phase and amplitude data fitting, respectively. For both types of samples and detection techniques used, the thermal diffusivity data was interpreted using the concept of effective thermal resistance for a series two-layer system. This model predicts that the thermal diffusivity of the composite sample depends not only on the thermal diffusivity of its constituent materials but also on the ratio of their thermal conductivities. The experimental data for both samples were adequately described by this effective sample model.

The above results also suggest a PA procedure for the complete characterization of the thermal diffusivity and conductivity of a sample. The method consists of using one of the PA techniques used above, say, the phase-lag method, for a two-layer system in which one of the layers is a standard material, such as, a thin plate glass for which both α and k are well known. The other layer consists of the test sample for which α and k are to be determined. By varying the standard layer thickness, we can make, for instance, three two-layer samples. Using the PA phase-lag technique we can then generate a set of data for α as function of $x = l_1/l$ (i.e., the ratio of the test sample thickness to the total system thickness). This data is then best fitted to Eq. (5) from which the values of the thermal diffusivities, as well as of the ratio λ of thermal conductivities of each component, are obtained. From the value of λ, the thermal conductivity of the test sample is readily found.

Since the phase-lag technique exhibits no explicit dependence on the absorbed power and surface conditions together with the fact that it is a single modulation frequency technique, the procedure outlined above for a two-layer system requires a minimum of measurements to be performed. In fact, all that is required is a set of five data points, namely, three for the two-layer system with varying thicknesses and two for the isolated components. We believe the accuracy together with its simplicity will render the proposed phase-lag method as a reliable and simple technique for the complete photoacoustic characterization of the thermal properties of solid samples. A similar procedure could also be adopted with the OPC detection technique.

ACKNOWLEDGMENTS

The authors are grateful to the Brazilian agencies Fundação de Amparo e Pesquisa Estado de São Paulo (FAPESP), Conselho Nacional de Desenvolvimento Científico e Tecnológico (CNPq), and Coordenação de Aperfeiçoamento de Pessoal do Ensino Superior (CAPES) for partial support of this work.

[1]H. Vargas and L. C. M. Miranda, Phys. Rep. **161**, 43 (1988).
[2]Y. S. Touloukian, R. W. Powell, C. Y. Ho, and M. C. Nicolasu, *Thermal Diffusivity* (IFI/Plenum, New York, 1973).
[3]G. Ziegler and D. P. H. Hasselman, J. Mater. Sci. **16**, 495 (1981).
[4]N. F. Leite, N. Cella, H. Vargas, and L. C. M. Miranda, J. Appl. Phys. **61**, 3023 (1987).
[5]A. Torres-Filho, L. F. Perondi, and L. C. M. Miranda, J. Appl. Pol. Sci. **35**, 103 (1988).
[6]B. Merté, P. Korpiun, E. Lüscher, and R. Tilgner, J. Phys. Colloq. **44**, 06-463 (1983).
[7]A. Torres-Filho, N. F. Leite, L. C. M. Miranda, N. Cella, and H. Vargas, J. Appl. Phys. **66**, 97 (1989).
[8]A. C. Bento, H. Vargas, M. M. F. Aguiar, and L. C. M. Miranda, Phys. Chem. Glasses **28**, 127 (1987).
[9]M. J. Adams and G. F. Kirkbright, Analyst **102**, 281 (1977).
[10]R. T. Swimm, Appl. Phys. Lett. **42**, 955 (1983).
[11]C. L. Cesar, H. Vargas, J. Mendes Filho, and L. C. M. Miranda, Appl. Phys. Lett. **43**, 555 (1983).
[12]A. Lachaine and P. Poulet, Appl. Phys. Lett. **45**, 953 (1984).
[13]O. Pessoa, Jr., C. L. Cesar, N. A. Patel, H. Vargas, C. C. Ghizoni, and L. C. M. Miranda, J. Appl. Phys. **59**, 1316 (1986).
[14]W. Karplus and W. W. Soroka, *Analog Methods* (McGraw-Hill, New York, 1959), p. 59.
[15]T. Tominaga and K. Ito, Jpn. J. Appl. Phys. **27**, 2392 (1988).
[16]A. Rosencwaig and A. Gersho, J. Appl. Phys. **47**, 64 (1975).
[17]D. Grzegorczyk and G. Feineman, *Handbook of Plastics in Electronics* (Reston, Reston, VA, 1974).
[18]H. S. Carslaw and J. C. Jaeger, *Conduction of Heat in Solids* (Clarendon, Oxford, 1973).
[19]M. D. Silva, I. N. Bandeira, and L. C. M. Miranda, J. Phys. E **20**, 1476 (1989).
[20]L. F. Perondi and L. C. M. Miranda, J. Appl. Phys. **62**, 2955 (1987).
[21]G. M.Sessler, J. Acoust. Soc. Am. **35**, 1354 (1963).
[22]G. M. Sessler and J. E. West, in *Electrets,* Vol. 33 of *Springer Series in Topics in Applied Physics,* edited by G. M. Sessler (Springer, Berlin, 1980), p. 347.
[23]P. M. Morese, *Vibrations and Sound* (McGraw-Hill, New York, 1948), p. 193.
[24]F. A. McDonald and G. C. Wetsel, Jr., J. Appl. Phys. **49**, 2313 (1978).
[25]A. Rosencwaig, *Photoacoustics and Photoacoustic Spectroscopy* (Wiley, New York, 1980).
[26]G. Rousset, F. Lepoutre, and L. Bertrand, J. Appl. Phys. **54**, 2383 (1983).
[27]W. J. Roff, J. R. Scott, and J. Pacitti, *Handbook of Common Polymers* (CRC, Cleveland, OH, 1971).